Available online at www.sciencedirect.com

ScienceDirect

Geochimica et Cosmochimica Acta 314 (2021) 209–222

Geochimica et Cosmochimica Acta

www.elsevier.com/locate/gca

Experimental study on Fe solubility in vapor-rich hydrothermal fluids at 400–500 °C, 215–510 bar: Implication for Fe mobility in seafloor vent systems

Yanlu Xing [a,*,1], Peter Scheuermann [a,b,*,1], William E. Seyfried Jr. [a]

[a] Department of Earth and Environmental Sciences, University of Minnesota, Minneapolis, MN 55455, USA
[b] Department of Earth, Ocean and Atmospheric Sciences, University of British Columbia, Vancouver, BC V6T 1Z4, Canada

Received 1 April 2021; accepted in revised form 20 September 2021; available online 24 September 2021

Abstract

In seafloor hydrothermal systems, vent fluids usually contain elevated dissolved iron (Fe) that is significantly enriched relative to deep ocean seawater. It is commonly thought that Fe is preferentially transported in dense Cl-rich fluids due to the formation of aqueous Fe-Cl complexes. However, Fe enrichment in vapor-rich low-density fluids with low Cl concentrations (<550 mmol/kg) underscores the efficacy of the low-Cl vapor-rich phase to transport Fe in both subaerial and submarine hydrothermal systems. Currently, transport of Fe in low-density vapor-rich fluids is poorly understood due to the lack of high temperature–pressure (T-P) solubility experiments and requisite thermodynamic data. Here, we report new data of Fe solubility from experiments conducted at 400–500 °C, 215–510 bar, targeting fluids with low-density (~0.1–0.35 g/cm^3). The experiments were performed in the KCl-H_2O system with hematite-magnetite and K-feldspar-muscovite-quartz as mineral buffering assemblages. Our results show that Fe solubility positively correlates with density and fluid chlorinity, which are affected by temperature and pressure. The equilibrium constants (log K_{hm}) for Fe-buffering reaction $Fe_3O_4(s) + 2HCl(aq) = Fe_2O_3(s) + FeCl_2(aq) + H_2O$ were determined. The new data and the data calculated using Helgeson-Kirkham-Flowers (HKF) equation of state were fit into a density model to extrapolate log K_{hm} for hematite-magnetite Fe buffering reaction over a wide T-P range. The density models for magnetite dissolution reaction and pyrite-pyrrhotite equilibrium were also fit based on HKF to allow redox constraints. We show that calculated Fe solubility are in good agreement with measured values in vapor-rich fluids formed via phase separation in mineral buffered and basalt alteration experiments at elevated T-P. The density model was further applied to model Fe transport in fluids at the Brandon hydrothermal field at East Pacific Rise (EPR) 21°S, with T-P constrained by Si-Cl geothermobarometer. The calculations suggest that the reported Fe concentrations of vent fluids at Brandon reflect phase separation occurring at depth in the seafloor, with T-P up to 450 °C, 400 bar, and redox conditions buffered by pyrite-pyrrhotite-magnetite equilibrium.

Keywords: Fe solubility; Vapor-rich fluids; Density model; Phase separation; Vent fluid; Brandon hydrothermal field

1. INTRODUCTION

Iron is one of the most abundant metals in natural hydrothermal systems and is thought to be predominantly transported as Fe chloride aqueous complexes in condensed Cl-rich fluids (Chou and Eugster, 1977; Ding and Seyfried, 1992; Fein et al., 1992; Ohmoto et al., 1994; Liu et al., 2006;

* Corresponding authors at: Department of Earth and Environmental Sciences, University of Minnesota, Minneapolis, MN 55455, USA (P. Scheuermann).
E-mail addresses: yanluxxing@gmail.com (Y. Xing), pscheuer@eoas.ubc.ca (P. Scheuermann).
[1] **Y.X.** and **P.S.** contributed equally to the completion of this study.

https://doi.org/10.1016/j.gca.2021.09.027
0016-7037/

Testemale et al., 2009; Brugger et al., 2016; Xing et al., 2019; Stefánsson et al., 2019). However, Fe enrichment in seafloor vent fluids with Cl concentration less than seawater is widely reported for modern seafloor hydrothermal systems (Butterfield et al., 1990; Ding and Seyfried, 1992; Edmonds et al., 1996; Seyfried et al., 2003; Von Damm et al., 2003; German and Seyfried, 2014; Pester et al., 2015; McDermott et al., 2018). Modern vent fluids are characterized by a wide range of salinity from below 50 mmol/kg to over 1000 mmol/kg Cl (Butterfield et al., 1990; Butterfield et al., 1994; Von Damm et al., 1995; Gamo et al., 1996; Seyfried et al., 2003; Gallant and Von Damm, 2006; Seyfried et al., 2011; McDermott et al., 2018). Lacking mineral phases that can act as a Cl sink, this wide range of fluid salinity relative to precursor seawater confirms the role of phase separation in the chemical evolution of seafloor hydrothermal vent fluids (Foustoukos and Seyfried, 2007; German and Seyfried, 2014). The surprisingly high Fe concentration in many of the Cl depleted vapor-rich vent fluids (up to > 10 mmol/kg Fe; by comparison, seawater has < 0.001 μmol/kg Fe; e.g., Von Damm et al., 1985; Seyfried et al., 2003; McDermott et al., 2018) indicates that such fluids cannot be discounted as a significant Fe transport agent, the relatively low dissolved Cl notwithstanding. However, the transport of Fe in vapor-rich low-density fluids remains poorly understood. Yet, the ubiquitous occurrence of Fe in such fluids in many important natural hydrothermal systems makes it critical to better constrain Fe transport in these conditions. These data are especially relevant to provide information critical to assess mass transfer during large scale hydrothermal processes, such as deep oceanic crust alteration and magmatic-hydrothermal ore formation.

Chloride is commonly known as the predominant ligand responsible for Fe transport in hydrothermal fluids. Important Fe-Cl complexes include Fe(II) species such as $FeCl^+$, $FeCl_2$(aq), $FeCl_3^-$ and $FeCl_4^{2-}$ that are usually the predominant species at elevated temperatures (>100 °C) (Heinrich and Seward, 1990; Ding and Seyfried, 1992; Testemale et al., 2009; Lemire et al., 2013; Brugger et al., 2016; Scholten et al., 2019; Xing et al., 2019), and Fe(III) species such as $FeCl^{2+}$, $FeCl_2^+$,$FeCl_3$(aq) and $FeCl_4^-$ that are more important at lower temperature (<100 °C), more oxidized near surface conditions (Liu et al., 2006; Scholten et al., 2019; Stefánsson et al., 2019). In low-density vapor-like fluids, neutral Fe(II)-Cl species such as $FeCl_2$(aq) or vapor components in the form of $FeCl_2{\cdot}nH_2O$ with n representing hydration number may be the predominant Fe species (Bischoff and Rosenbauer, 1987; Simon et al., 2004; Pokrovski et al., 2005a; Pokrovski et al., 2008; Kokh et al., 2016). Although a relationship between vapor/fluid chlorinity and Fe solubility at elevated temperatures and pressures has been suggested (e.g., Simon et al., 2004; Pokrovski et al., 2005a; Pester et al., 2015), limitations of available thermodynamic data effectively preclude quantitative evaluation of Fe transport in various T-P-x conditions of interest to a wide range of geochemical systems (Pokrovski et al., 2013).

Hence, measurement of Fe solubility in fluids with relatively low to intermediate densities at elevated T-P conditions is important to understand Fe transport and its response to various factors, such as P, T, redox, and fluid salinity, where low-density vapor-rich fluids can be predominant, such as seafloor vent systems. These data also provide key information regarding fluid-rock interaction processes more broadly in deep oceanic crust. Here, we report new data on Fe solubility in vapor-rich, low-density fluids, through laboratory phase separation experiments conducted at 400–500 °C, 215–510 bar in a KCl-H_2O and K-Feldspar-muscovite-quartz-hematite-magnetite system. H_2S was not considered in our experiment because its concentrations are commonly much lower than that of Cl in seafloor vent systems (Diehl and Bach, 2020). The experimental data were used to determine the equilibrium constants for Fe solubility reaction in low-density vapor-rich fluids. The empirical density model was fit based on the new experimental data and the equilibrium constants calculated with the HKF equation of state (EoS). Density models for magnetite solubility reaction and pyrite-pyrrhotite equilibrium were also fit based on HKF EoS for aqueous species as a means of comparison and to constrain the redox effects. Predictions of Fe solubility using the new data show good agreement with data from previous experiments and field observations. Thus, the results reported in the present study provide new insights on quantitative understanding of the effects of T-P and fluid chemistry on Fe transport during phase separation and fluid-rock interactions in seafloor hydrothermal systems.

2. METHODOLOGY

2.1. Experiments

Experiments were conducted using a fixed volume (150 ml) titanium hydrothermal reactor (Scheuermann et al., 2018; Fowler et al., 2019). The cone seal reactor is made of high-strength Ti-alloy that is capable of high temperature–pressure experiments up to 500 °C, 510 bar. The interior surface of the reactor was passivated with 20 wt% nitric acid at 300 °C for 10 hours following the procedure described in Fowler et al. (2019). This passivation process allows formation of an inert TiO_2(s) coating on all wetted internal surface, so as to inhibit possible reaction with included redox and pH buffers. The effectiveness of this treatment has been demonstrated by Fowler et al. (2019) via injecting a known amount of H_2 into a passivated Ti-alloy reactor at same conditions and measuring the fluid concentration periodically over five days. As was reported by Fowler et al. (2019), no change in the dissolved H_2(aq) concentration was found within error, indicating that Ti-alloy does not participate in reactions involving H_2(aq) after passivation.

The hematite-magnetite (HM) mineral assemblage was used to buffer redox, while also acting as a source of Fe. pH buffering was provided by K-feldspar-muscovite-quartz (KMQ) assemblage together with constraints imposed by K-bearing fluid composition. Approximately 5–7 g of each mineral was added to the reactor, amounts sufficient for requisite buffering reactions relative to total solution volume of the reactor. The starting solution was

prepared using reagent grade KCl and deionized water, with the KCl concentration adjusted to be ~ 1000 mmol/kg. It is noted that we used KCl-H_2O fluids instead of NaCl-H_2O to maintain consistency between the composition of the fluid and minerals (e.g., K-feldspar) and to avoid reactions involving Na-K solid solutions.

Immediately prior to loading minerals and fluids into the reactor, ultrapure argon gas was flushed for 20 minutes to expel dissolved O_2. Moreover, ~200 μmol/kg formic acid (CH_2O_2) was added to the staring fluid. Formic acid decomposes into H_2 and CO_2 at T > 250 °C (McCollom and Seewald, 2003; Pester et al., 2015), providing an additional mechanism to remove dissolved O_2 in the initial stage. A 1/16″ Ti-sheathed type E thermocouple (Chromel-Constantan) was inserted into the reactor with direct contact with the fluid reactant to directly and precisely monitor the solution temperature (Fig. 1a). The thermocouple has an accuracy of ± 1.5 °C and was calibrated before the experiment using a dry block probe calibrator (Omega Hot Point®). A Teledyne ISCO syringe pump was used to control system pressure, which can reach up to a maximum of 517 bar. The syringe pump was connected to the reactor via a piston separator, composed entirely of titanium alloy for requisite corrosion resistance. Thus, fluid can be added or withdrawn during an experiment, while pressure is maintained constant (±0.1 bar). During the experiment, the autoclave was positioned at a slight angle above horizontal (gas sampling valve at upper side; see Fig. 1a), in order to promote vapor and liquid segregation, as well as minimizing temperature gradients along the long axis of the reactor. Experiments started at lowest pressure of each isothermal series and the pressure was increased after each sample extraction. For each T-P condition, the entire system was allowed sufficient time to achieve equilibrium: a minimum of 4 days at 400 and 425 °C, and 3 days at 450 °C and 500 °C, consistent with previous studies on silicate-fluid and Fe-oxide-fluid equilibrium at similar conditions (Kishima and Sakai, 1984; Foustoukos and Seyfried, 2007; Scheuermann et al., 2020).

During sampling, ~0.3 g fluid was removed to flush the capillary line, before acquiring fluid derived entirely from within the reactor at experimental conditions. Because the reactor was positioned with a slight angle, vapor and liquid phases were allowed to be segregated effectively during sampling. This ensures the sampled vapor fluids via the capillary line at the upper side of the system are genuinely vapor phase without contamination from the remaining liquid phase. The aliquots for cation analysis were diluted with 1 M ultrapure HCl to prevent Fe precipitation. The aliquots for H_2(aq) analysis were collected using a gas-tight syringe attached with a gas-tight Teflon valve. Additional aliquots were taken for $pH_{25°C}$ measurement and anion analysis. After the experiment, the solid mineral phases inside the reactor were collected for powder X-ray diffraction (XRD) analysis to confirm the consistency of the buffering minerals.

2.2. Analytical Procedures

The solution $pH_{25°C}$ was measured immediately after sampling, using a ThermoRoss micro-electrode, with an uncertainty of ± 0.1 pH units. The pH electrode was calibrated using standard pH buffers with $pH_{25°C}$ 4, 7, and 10 before each measurement. The concentration of Fe, K,

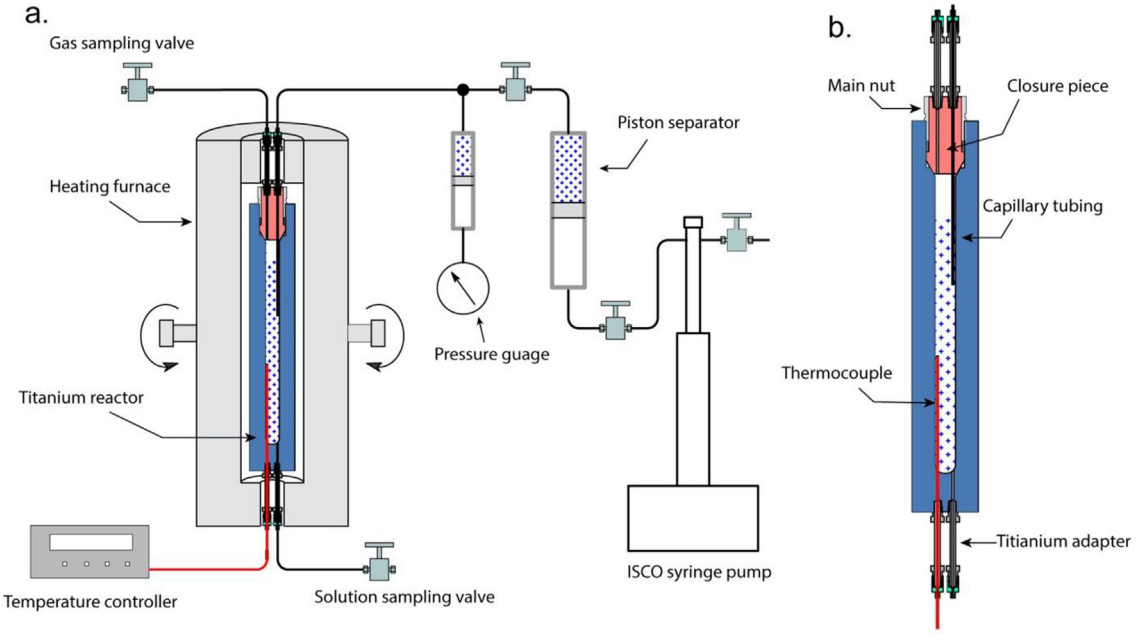

Fig. 1. Illustration of the reactor and the experimental setup. (a) Conceptual diagram showing the experimental system. Phase separation was simulated by monitoring pressure via ISCO syringe pump. The reactor was placed with a tilted angle that vapor-like phase was at the upper side of the reactor, whereas the fluid phase was at the lower side. Gas samples were collected via the gas sampling valve. (b) Detailed view of the reactor. Thermocouple was inserted into the solution for accurate control of temperature.

Na and SiO_2(aq) was analyzed using an ICAP-6500 inductively coupled plasma optical emission spectroscopy (ICP-OES). The concentration of Cl was analyzed by ion chromatography (IC). Samples measured by ICP-OES were analyzed three times and those measured by IC were run twice. Uncertainties for ICP-OES and IC measurements are 3% and 2%, respectively. The concentration of H_2(aq) was measured by an Agilent 6980 gas chromatography (GC) equipped with a carbon molecular sieve column (Carboxen™ 1010 PLOT) and a thermal conductivity detector. The GC data was calibrated with a gas standard containing 1% H_2 gas before analysis.

Minerals collected before and after the experiment were acid digested and analyzed for chemical composition with ICP-OES. For the acid digestion, the minerals were firstly powdered, and then weighed for ~ 0.1 g and mixed with a 10 mL mixture of HF, HNO_3, and deionized water in a sealed Teflon cylinder. The digestion was allowed for 2 hours at 200 °C. Standard rock samples (BHVO-1 and G-2) provided by the United States Geological Survey (USGS) were digested and analyzed concurrently with the experimental samples as reference standards. The USGS standards returned within ± 10% of the stated values of the major oxides.

The XRD patterns of minerals were collected on a Rigaku Miniflex© X-ray diffractometer with cobalt radiation (Co-Kα1 radiation, λ = 1.78892 Å). Phase identification and Rietveld refinement was conducted using Match! software package. Crystal structure data of minerals were collected from the COD database.

3. RESULTS

The chemistry of the fluid samples from the experiment are summarized in Table 1. The results show that composition of the low-density vapor-rich fluids is characterized by significantly lower dissolved Fe, K, SiO_2(aq) and Cl, but higher H_2. The Fe and Cl concentrations in the vapor-rich fluids increase with pressure for a given temperature (Fig. 2). Such correlation for Fe and Cl concentration with pressure indicates coupled Fe and Cl behavior in these fluids.

Density has been emphasized as an important factor controlling metal partitioning of vapor–liquid equilibria (Pokrovski et al., 2005a; Pester et al., 2015). In the present study, the vapor/fluid density was calculated using equations reported by Driesner and Heinrich (2007). Their empirical parameters allow for calculation of volumetric properties for the fluids. We further used the molar weight of KCl in the density calculation equation to obtain the optimum fluid density for KCl-H_2O system of our experiment (Table 1). Such treatment yields agreement within 10% of experimental measurements of KCl-H_2O density at hydrothermal conditions, 300–700 °C, 800–2000 bar (Khaibullin and Borisov, 1966; Bodnar and Sterner, 1985). The fluid data were plotted in Fig. 3b. As shown, a linear correlation was observed for Fe solubility and fluid density. Such correlation can be described using the empirical equation:

$$\log\ m(\mathrm{Fe}) = 4.79(\pm 0.19) + 4.14(\pm 0.33)\log\rho, \mathrm{Adj.}R^2 = 0.902 \quad (1)$$

Table 1
Chemical composition of experimental samples.

T	P	Phase	Density†	H_2	$pH_{25\ °C}$	Fe	K	Cl	Na	$SiO_{2(aq)}$
(°C)	(bar)		g/cm^3	(μmol/kg)		(μmol/kg)	(mmol/kg)	(mmol/kg)	(mmol/kg)	(mmol/kg)
400	215	V	0.116	1222	3.86	21	11.2	13.3	0.01	1.4
400	240	V	0.150	545	3.53	23	15.16	16.32	0.067	2.37
400	260	V	0.193	372	3.60	36	25.62	27.22	0.116	3.11
400	280	L	0.517	145	4.10	2554	674	659	2.68	13.96
400	330	L	0.604	40	4.2	3853	931	1012	4.06	21
425	322	V	0.240	294	3.26	90	80	79	0.12	5.14
425	335	V	0.341	219	2.39	1100	383	390	0.62	9.84
425	338	V	0.415	236	3.58	2040	618	602	0.95	13.64
450	350	V	0.205	890	3.55	46	43	45.24	0.176	5.8
450	380	V	0.253	519	3.06	202	93	96	0.88	7.9
450	400	V	0.297	346	3.09	606	187	183.16	1.52	10.5
450	415	V	0.381	300	3.63	1393	528.9	534.97	1.689	15.57
450	430	L	0.451	131	3.09	5782	800	826.6	5.9	20.9
450	470	L	0.488	127	3.43	5464	790	819.3	5.55	21.7
500	400	V	0.203	4237	3.03	92	31	33	0.099	6.95
500	430	V	0.238	2210	3.03	76	49	52	0.168	7.88
500	470	V	0.281	1650	3	166	83	87	0.319	10.15
500	510	V	0.265	1206	2.95	506	173	182	0.629	12.88

Concentration of elements indicates the solution composition relative to vapor/liquid.
V = vapor-rich fluid; L = dense liquid fluid.
† The densities of vapor-rich fluid and co-existing liquid fluids are calculated based on Driesner and Heinrich (2007) with modifications made to account for KCl-H_2O system.

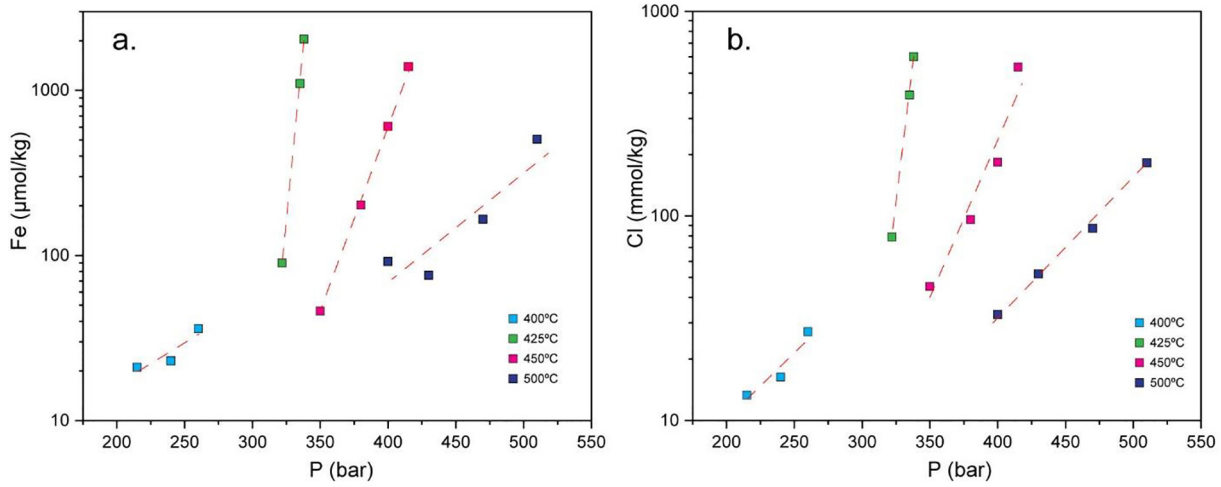

Fig. 2. Measured concentration of Fe (μmol/kg) and Cl (mmol/kg) relative to pressure (P, bar) in vapor-like fluids. (a) Fe solubility as a function of pressure. (b) Cl concentration as a function of pressure. Dashed lines represent the linear trend line. y axis in (a) and (b) are in logarithm scale.

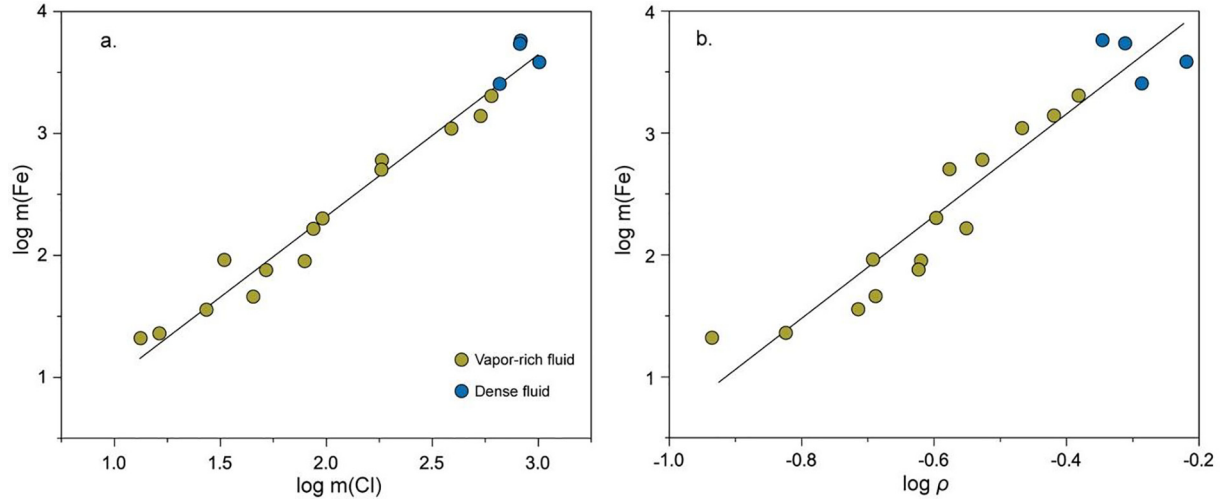

Fig. 3. Fe concentration (μmol/kg) vs. Cl (mmol/kg) and fluid density, ρ (g/cm^3). (a) log m(Fe) - log m(Cl). (b) log m(Fe) -log ρ. Black solid lines represent linear fitting. In (a), the equation of linear fitting is: log m(Fe) = -0.29(±0.13) + 1.31(±0.06) · log m(Cl), Adj.R^2 = 0.969.

where m(Fe) represents Fe concentration, μmol/kg; ρ is the fluid density, g/cm^3; Adj.R^2 is the adjusted R-square. The 1σ error of the fitted coefficients was estimated by least-squares regression of the experimental data.

XRD analyses document the presence of hematite and magnetite in the mineral assemblage after the experiment (Supplementary Figs. S1 and S2). The chemistry of hematite and magnetite also confirm that the chemical composition of both minerals remained constant during the experiment (Supplementary Table S1), providing redox buffering effects as required. The fH_2 was also calculated for fluid samples of our experiment (see more details in the discussion; Table S8).

4. DATA TREATMENT

4.1. Fe speciation

Metal transport in subcritical and supercritical fluids at elevated T-P conditions has been commonly attributed to (electrically) neutral species (Simon et al., 2004; Pokrovski et al., 2005a; Williams-Jones and Heinrich, 2005; Hurtig and Williams-Jones, 2014; Mei et al., 2014; Hurtig and Williams-Jones, 2015; Kokh et al., 2016). Despite the complexity of Fe(II/III)-Cl complexation has been recognized in dense Cl-bearing fluids, the neutral $FeCl_2$(aq) or $FeCl_2 \cdot nH_2O$ has typically been used to account for Fe

transport in Cl-bearing fluids with relatively low to intermediate densities at elevated T-P, based on abundant and largely consistent experimental and theoretical data (Chou and Eugster, 1977; Boctor et al., 1980; Bischoff and Rosenbauer, 1987; Heinrich and Seward, 1990; Ding and Seyfried, 1992; Fein et al., 1992; Simon et al., 2004; Pokrovski et al., 2008; Lemire et al., 2013; Kokh et al., 2016). Other neutral species could be significant in certain circumstances depending on bulk fluid chemistry and T-P conditions. For example, the neutral Fe(II) hydroxide species, e.g., $Fe(OH)_2$(aq) or $Fe(OH)_2{\cdot}nH_2O$, may be important for Fe transport in Cl-free systems and/or alkaline fluids (Tremaine and LeBlanc, 1980; Ziemniak et al., 1995), yet their role in Cl-dominant, acidic fluids seems improbable. The study by Kokh et al. (2016) inferred the possible importance of Fe-HS species in H_2S-rich vapor. However, the stoichiometry and stability of such species are still unknow due to the lack of experimental and/or spectral data. The sulfur-rich vapor of Kokh et al. (2016) have H_2S contents (>0.1 m H_2S) that are significantly higher than vent fluids in mid-ocean ridge (MOR) hydrothermal systems (commonly < 0.01 m H_2S in vent fluids; Diehl and Bach, 2020). Owing to the high of Cl/H_2S, Fe-Cl species are suggested to be the predominant species in MOR systems (e.g., Bischoff and Rosenbauer, 1987). As illustrated in Fig. 3a, both vapor-like fluids and the dense liquid phase in our experiment when present, are well aligned in their Fe-Cl compositions, suggesting consistency of Cl stoichiometry and speciation for Fe-Cl complexes in these fluids. Hence, $FeCl_2$(aq) is considered as the predominant Fe species in fluids of our experiment, in line with the previous experimental studies on Fe solubility in Cl-dominant subcritical-supercritical hydrothermal systems (Bischoff and Rosenbauer, 1987; Simon et al., 2004; Pokrovski et al., 2005a; Pokrovski et al., 2008).

4.2. Development of the density model

For thermodynamic extrapolation of equilibrium constants of key solubility reactions, the widely used HKF EoS requires water density above 0.35 g/cm^3 (Tanger and Helgeson, 1988; Johnson and Oelkers, 1992), which prevents the application of this model to the T-P range of the present study, where water density often falls below this limit (Table 1). Instead, a density model incorporating macroscopic parameters, i.e., temperature and pure water density, was usually adopted as a means to estimate and extrapolate equilibrium constants of the Fe-solubility controlling reactions over a wide range of T-P conditions in a manner consistent with previous interpretation of experimental and theoretical data (Anderson et al., 1991; Manning, 1994; Pokrovski et al., 2013). This approach has been successfully applied in several solubility studies reaching the low-density regime where HKF is not applicable (Anderson et al., 1991; Manning, 1994; Pokrovski et al., 2005b; Manning, 2013; Pokrovski et al., 2013; Scheuermann et al., 2018; Zotov et al., 2018; Scheuermann et al., 2019). Alternatively, a vapor model involving hydration number in neutrally charged metal complexes has been developed in several recent studies to interpret the solubility data for metals such as Ag, Cu and Mo in the vapor-like fluids (Migdisov and Williams-Jones, 2013; Hurtig and Williams-Jones, 2014, 2015; Velizhanin et al., 2020). However, the hydration number of such vapor metal complexes changes with vapor/fluid density (Mei et al., 2014; Lemke and Seward, 2018), and it commonly requires supporting solubility data at various T-P conditions to more effectively regress requisite hydration parameters and component stoichiometry (Williams-Jones and Heinrich, 2005; Migdisov and Williams-Jones, 2013; Pokrovski et al., 2013; Hurtig and Williams-Jones, 2014, 2015; Velizhanin et al., 2020). The empirical EoS model developed by Akinfiev and Diamond (2003) is an alternative that is capable of well-predicting thermodynamic properties of neutral species at low-density vapor-like fluids, which however requires determination of several adjustable empirical parameters from abundant experimental data and good knowledge of ideal gas/vapor speciation/thermodynamics.

In the present study, the density model as outlined above was adopted to estimate the equilibrium constants of the Fe solubility reaction (reaction [2]). There are several advantages of the density model as it: (i) allows estimation of equilibrium constants for reactions when limited solubility data are available; and, (ii) avoids the complexity of the hydration number as required for the vapor model. We follow the line of reasoning from numerous other studies in support of $FeCl_2$(aq) as the predominant Fe-bearing species for the development of the density model.

The Fe solubility reaction in our experiment is expressed as:

$$Fe_3O_4(s) + 2HCl(aq) = Fe_2O_3(s) + FeCl_2(aq) + H_2O,\ K_{hm} \quad (2)$$

where K_{hm} is the equilibrium constant that is calculated as:

$$\log K_{hm} = \log a(FeCl_2) - 2\log a(HCl) \quad (3)$$

$a(FeCl_2)$ and $a(HCl)$ denote the activity of $FeCl_2$(aq) and HCl(aq), and are calculated as:

$$a(FeCl_2) = \gamma_{FeCl2}\ m(FeCl_2) \quad (4)$$

$$a(HCl) = \gamma_{HCl}\ m(HCl) \quad (5)$$

$m(FeCl_2)$ and $m(HCl)$ are the molal concentration of $FeCl_2$(aq) and HCl (aq), with γ_{FeCl2} and γ_{HCl} denoting their activity coefficients, respectively. For neutral species, their activity coefficients were taken as 1 (Manning, 1994; Anderson, 2005; Manning, 2013; Scheuermann et al., 2019).

Values of $m(FeCl_2)$ were estimated from measured Fe concentration taking $FeCl_2$(aq) as the predominant species (Table 2). m(HCl) was estimated from pH measurements assuming HCl(aq) is the predominant species at in-situ T-P conditions, which fully decomposes to H^+ and Cl^- upon quenching at 25 °C (Table 2). This is supported by calculations of the association constants of HCl(aq) based on data provided by Ho et al. (2001), showing strong stability of neutrally charged HCl(aq), indicating the predominance of HCl(aq) rather than H^+ at in-situ conditions of the experiments (see Table S2 for calculated association constants for HCl(aq)). Similarly, KCl(aq) also shows strong

Table 2
Parameters for calculation of log $K_{hm.}$

T, °C	P, bar	Water density, g/cm^3	m(HCl), mmol/kg H_2O	m($FeCl_2$), μmol/kg H_2O	log K_{hm}
400	215	0.116	0.14	21	3.04
400	240	0.149	0.30	23	2.42
400	260	0.189	0.25	36	2.76
425	322	0.229	0.55	90	2.47
425	335	0.257	4.07	1100	1.82
425	338	0.263	0.26	2041	4.47
450	350	0.202	0.28	46	2.76
450	380	0.242	0.87	202	2.43
450	400	0.271	0.81	606	2.96
450	415	0.293	0.23	1393	4.40
500	400	0.178	0.93	92	2.02
500	430	0.200	0.93	76	1.94
500	470	0.232	1.00	166	2.22
500	510	0.266	1.12	506	2.60

stability and is the predominant species accounting for potassium concentration at the experimental conditions (Table S2 shows the association constants for KCl(aq); Ho and Palmer, 1997). Therefore, during the experiments, reaction that buffers HCl(aq) can be expressed as:

$$3KAlSi_3O_8(s) + 2HCl(aq) = 2KCl(aq) + KAl_3Si_3O_{10}(OH)_2(s) + 6SiO_2(s) \quad (6)$$

The experiment setup allows the measured composition of collected fluids to be representative of that at experimental conditions (Ding and Seyfried, 1992; Scheuermann et al., 2020). The rapid sampling capability notwithstanding, special emphasis was placed on pH measurement, which was performed immediately. This was done to more effectively preclude the possibility of quench effects on pH determination. Therefore, HCl(aq) formed at the in-situ conditions of the experiment contributes to the measured $pH_{25°C}$, and thus m(HCl) can be well estimated from this approach.

The density model proposed by Anderson et al. (1991) includes seven T-P independent parameters, which are ultimately related to specific thermodynamic variables involved in the reaction. Accurate determination of these parameters requires T-P data sufficient for full regression of all parameters as defined. A more simplified version of the fully developed density model, however, has been suggested to be capable of describing thermodynamic properties of solubility reactions of minerals with good accuracy (Pokrovski et al., 2005b; Zotov et al., 2018). Thus, we applied a 2-parameter model involving water density for the mineral buffered Fe-solubility reaction (reaction [2]). Efforts were made to fit the data into density models with additional parameters. However, owing to limitations of the range in experimental data, our attempts to fit a greater number of parameters show no significant improvement compared to the 2-paramter fitting. Therefore, the 2-parameter density model was adopted. Experimental data were linked with equilibrium constants at 300 to 500 °C, 100–800 bar calculated with HKF EoS (Supplementary Table S3, S4 and S5) for fitting where model applies. It is important to note that despite the capability of HKF for extrapolating equilibrium constants of neutral or charged species in fluids with density above 0.35 g/cm^3, the uncertainties of such extrapolations can be significant at conditions within the critical region of water due to uncertainties imposed on thermodynamic parameters intrinsic to the HKF EoS (Johnson and Oelkers, 1992). Moreover, it is noted that two experimental data points, at 425 °C, 338 bar, and 450 °C, 415 bar, are sufficiently close to the two-phase boundary of the starting KCl-H_2O solution to render the physical conditions uncertain. Therefore, these two data points were excluded from the dataset used for model fitting. The HKF EoS data used were derived from an updated version of the SUPCRT database, with details on the source of the thermodynamic data provided in Table S3. In particular, HKF parameters of $FeCl_2$(aq) were from Sverjensky et al. (1997); HKF parameters of HCl(aq) were from Tagirov et al. (1997).

Accordingly, the density model is

$$\log K_{hm} = 5.19(\pm 0.08) + 3.83(\pm 0.21) \cdot \log\ \rho_w, \mathrm{Adj.R}^2 = 0.873 \quad (7)$$

ρ_w is pure water density (g/cm^3).

Fig. 4a shows the log K_{hm} calculated from the experimental data and the density model. The predictions using the density model are in good agreement with the experimental data and the values calculated based on HKF. Although the density model is able to be fitted independently from the new solubility data, comparison with equilibrium constant calculated with HKF in mediate-high density fluids and including such data into the fitting can not only examine the reliability of the assumed speciation model (e.g., $FeCl_2$(aq)) but also serve to improve the fitting quality and extend the applicability of the density model to a wide T-P-density conditions. At the low-density range, deviations between the density model and the experimental data are likely the results of experimental uncertainties concerning the extremely difficult conditions for the samples to be experimentally produced, as well as uncertainties of thermodynamic properties of other species involved.

Linear extrapolation of equilibrium constants calculated based on HKF has been suggested as applicable to the low-density region for certain reactions (e.g., anhydrite solubility, Scheuermann et al., 2019; quartz solubility, Manning,

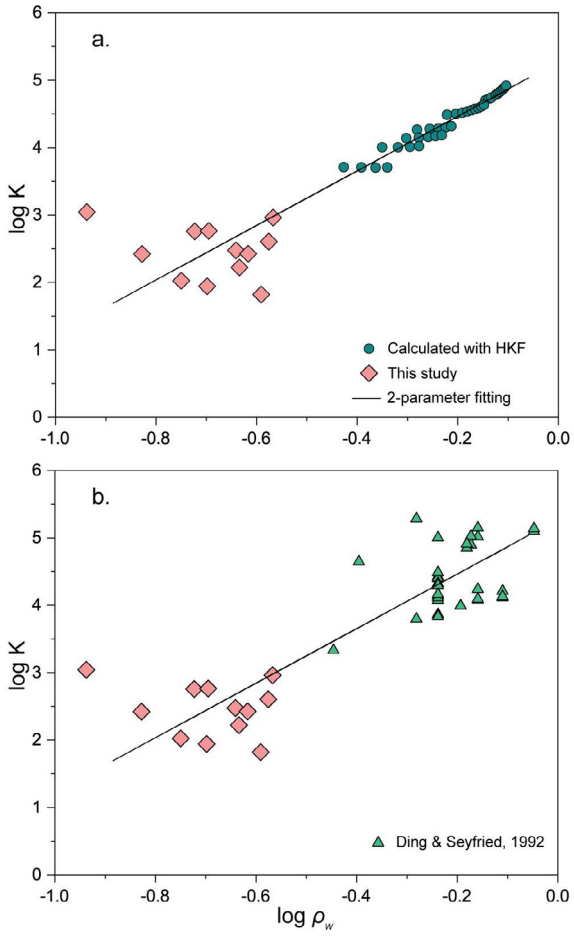

Fig. 4. Diagram showing log K *vs.* log ρ_w for Fe solubility reaction buffered by HM. (a) log K calculated with the experimental data and HKF are compared with the density model. In particular, the HKF EoS of aqueous species used for calculation were from Sverjensky et al. (1997) for $FeCl_2$(aq) and Tagirov et al. (1997) for HCl(aq). (b) log K calculated with the experimental data and the data by Ding and Seyfried (1992). The density model is expressed by the solid line.

1994). However, the appropriateness of such extrapolation for other solubility reactions has yet to be rigorously tested with experimental data. In the case of the HM buffered Fe solubility reaction (reaction [2]), we show that the density model (equation [7]) predicts values that are in good agreement with the experimental data (Fig. 4).To further test the capability of this model to a wide T-P, we calculated the log K_{hm} of reaction [2] for the experimental data of Ding and Seyfried (1992) who measured Fe solubility in HM buffered NaCl-H_2O fluids (0.03 to 1.24 m NaCl) at 200 to 450 °C and pressure from 300 to 500 bar. The calculation of log K_{hm} followed equations [3–5]. We found that these data, too, agree well with predictions from the simplified density model (Fig. 4b), lending strength to the usefulness of this approach. Thus, above results suggest that the simple density-based model is capable of providing reasonable extrapolation of equilibrium constants for solubility reactions over a relatively wide T-P range in fluids at supercritical-subcritical conditions where experimental data are extremely limited.

5. DISCUSSION

5.1. Effects of redox

The empirical density-based models utilized herein allow prediction of Fe solubility in fluids with low-intermediate density under pH and redox (HM) buffered conditions. However, Fe solubility is sensitive to redox constraints more generally, as has been reported in many studies (e.g., Bischoff and Rosenbauer, 1987; Ding and Seyfried, 1992; Xing et al., 2019). In natural seafloor hydrothermal systems, where fluid chemistry is predominantly buffered by altered basalt-fluid equilibria, reactions that control the Fe solubility and the system redox likely vary between the more oxidizing, HM equilibrium and the more reducing, pyrite-pyrrhotite-magnetite (PPM) equilibrium (Bischoff and Rosenbauer, 1987; Seyfried and Ding, 1995; German and Seyfried, 2014; Scheuermann et al., 2020). Therefore, the effects of fluid redox conditions need to be accounted for to meet more broadly based applications. To accomplish this, the Fe buffering reactions were extended to include magnetite solubility and pyrite-pyrrhotite equilibrium, as follows:

$$Fe_3O_4(s) + H_2(g) + 6HCl(aq) = 3FeCl_2(aq) + 4H_2O,\ K_{mgt} \quad (8)$$

$$2FeS(s) + 2HCl(aq) = FeS_2(s) + FeCl_2(aq) + H_2(g),\ K_{pp} \quad (9)$$

where K_{mgt} and K_{pp} are equilibrium constants for reactions [8] and [9], respectively. As shown for the HM buffer (reaction [2]), the simplified density model (equation [7]) is able to predict Fe solubility in low-density fluids (Fig. 4). Hence, this approach is used to extrapolate K_{mgt} and K_{pp} to the low-density region where HKF EoS for aqueous species is not directly applicable. For fitting of the density model, K_{mgt} and K_{pp} in fluids with density > 0.35 g/cm^3 (300–500 °C, 300–800 bar) were calculated (Tables S6 and S7) based on an updated SUPCRT database. In particular, the thermodynamic data for H_2(g) were based on Peng-Robinson-Stryjek-Vera (PRSV) EoS (Stryjek and Vera, 1986; Proust and Vera, 1989); thermodynamic data for minerals were from Holland and Powell (2011) (Table S3).

The results are as following:

$$\log K_{mgt} = 17.73(\pm 0.21) + 11.86(\pm 0.80) \cdot \log \rho_w, \text{Adj.R}^2 = 0.879 \quad (10)$$

$$\log K_{pp} = 5.09(\pm 0.03) + 2.75(\pm 0.13) \cdot \log \rho_w, \text{Adj.R}^2 = 0.932 \quad (11)$$

5.2. Prediction of Fe solubility

The newly determined density models were tested by comparing predicted m($FeCl_2$) with data reported in earlier experimental studies of Bischoff and Rosenbauer (1987) and Foustoukos and Seyfried (2007). The study of Bischoff and Rosenbauer (1987) involved phase separation

of seawater coexisting with basalt to buffer key aspects (e.g., metal contents, pH, fH_2) of the evolving vapor and liquid. Foustoukos and Seyfried (2007) investigated the effects of phase separation on Fe and volatile species, i.e., H_2 and H_2S, transfer by performing experiments at T-P conditions that are analogous to Bischoff and Rosenbauer (1987), but using PPM assemblage to provide requisite buffering of key aqueous and gaseous species. These experimental studies reported well-controlled T-P for fluid-vapor equilibria and chemical composition of the low-density vapor-rich fluid that is ideal for calculation of $m(FeCl_2)$ and comparison with measured data. In particular, the data by Foustoukos and Seyfried (2007) allow direct testing of the HKF-based density model for reactions [8] and [9] as PPM were used in their experiments.

Hence, at different redox conditions, the Fe solubility can be calculated as follows:

Hematite-magnetite buffering reaction (reaction [2]),

$$\log m(FeCl_2) = \log K_{hm} - 2\log m(HCl) \quad (12)$$

Magnetite dissolution reaction (reaction [8]),

$$\log\ m(FeCl_2) = (\log K_{mgt} + 6\log\ m(HCl) + \log\ fH_2)/3 \quad (13)$$

Pyrite-pyrrhotite equilibrium (reaction [9]),

$$\log\ m(FeCl_2) = \log K_{pp} + 2\log\ m(HCl) - -\log fH_2 \quad (14)$$

where fH_2 is the fugacity of H_2(g). fH_2 can be calculated from measured dissolved H_2(aq) ([H_2(aq)]) when available, via $Y_{H2\text{-}Cl}$ values reported in Scheuermann et al. (2020) with $Y_{H2\text{-}Cl} = fH_2$ / [H_2(aq)] for NaCl (or KCl) dominant fluids. Values of $Y_{H2\text{-}Cl}$ were calculated from temperature T (°C) and fluid density ρ (g/cm^3) using the empirical equation reported by Scheuermann et al. (2020):

$$\ln Y_{H^2-Cl} = 7.651 - 0.001214T + 0.0626\ln\rho + 0.00736T\ln\rho + 0.3876(\ln\rho)^2 \quad (15)$$

The calculated fH_2 for data from Bischoff and Rosenbauer (1987) and Foustoukos and Seyfried (2007) are provided in Table S9.

The predicted Fe concentrations are compared with the measured data in Fig. 5. It is shown that the measured data of Foustoukos and Seyfried (2007) are mostly close to values predicted for the PP buffer. The observed uncertainty is likely the result of uncertainties of fH_2 values (e.g., O_2 contamination, pH uncertainties), or Fe precipitation during sampling. But overall, the result is in good agreement with the experiment for which PPM mineral assemblage was used as the Fe source and redox buffer. Regarding data of Bischoff and Rosenbauer (1987), our calculations show that measured m(Fe) is between PP and HM buffers, in agreement with their experimental conditions. Thus, the results show that the empirical density model used to constrain the Fe solubility under various redox and P-T conditions for vapor-like fluids with relatively low-density (~0.1–0.35 g/cm^3), effectively expands the usefulness of predictions rooted in thermodynamic data ultimately derived from the HKF model, at conditions for which it rigorously

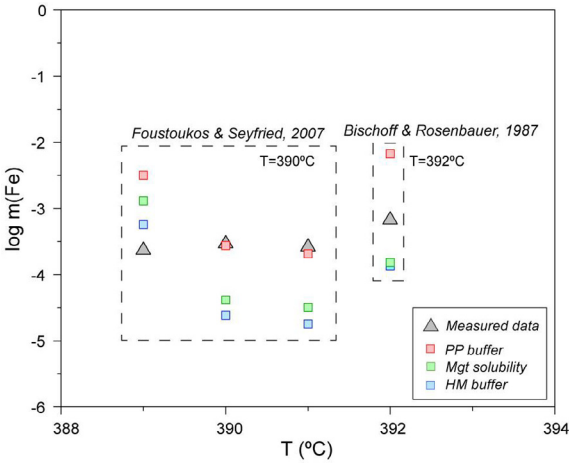

Fig. 5. Comparison of measured solubility of Fe (molal), i.e., m (Fe), with values predicted from the density model. Here we show the experimental data from studies of Bischoff and Rosenbauer (1987) for seawater-basalt experiment at 392 °C, 251 bar, and Foustoukos and Seyfried (2007) for equilibrium of NaCl-H_2O with PPM at 390 °C and 241–254 bar.

applies. Moreover, this quantitative understanding of Fe solubility also provides a possibility of using Fe as an additional indicator of redox and mineral assemblages that control fluid chemistry in various geological hydrothermal systems.

5.3. Applications to seafloor hydrothermal system

The apparent success of the application of the density model to other experimental systems encourages more challenging applications intrinsic to seafloor hydrothermal vents where phase separation effects and dissolved chemistry of Fe-rich vapors are well recognized. The Brandon hydrothermal field is located at the southern East Pacific Rise (21.5°S, EPR) with vent fluids reaching temperatures up to 405 °C (Von Damm et al., 2003). The physical conditions were measured to be 405 °C and 287 bar at the time of sampling, near the critical point of seawater (407 °C and 298 bar). Von Damm et al. (2003) suggested that phase separation at Brandon occurs at/near seafloor, given that the Cl concentrations of vent fluids (down to 297 mmol/kg) deviate moderately from seawater (~550 mmol/kg). However, calculations based on equations of Driesner and Heinrich (2007) indicate that higher T-P conditions, rather than 405 °C and 287 bar, are required to generate the dissolved Cl as observed at Brandon. This implies that phase separation may have actually occurred at deeper levels in the ocean crust. To predict Fe solubility in these vent fluids, the T-P conditions need to be better constrained. The solubility of quartz, i.e., SiO_2(aq), combined with dissolved Cl concentration, can be used to estimate T-P conditions of the subsurface phase separation in basalt-hosted seafloor hydrothermal systems, known as Si-Cl geothermobarometer (Foustoukos and Seyfried, 2007; Fontaine et al., 2009; Scheuermann et al., 2018). Foustoukos and Seyfried (2007) who applied a revised Si-Cl correlation, provided

an estimate of T-P conditions, suggesting that phase separation occurred at deeper levels, up to 420 °C and 320 bar. Recently, Scheuermann et al. (2018) performed new experiments measuring quartz solubility at elevated T-P conditions. These new solubility data show that the density equation of Fournier (1983) predicts quartz solubility that can well match the experimental data over a wide T-P and salinity range. We therefore applied the Si-Cl geothermobarometer to Brandon vent fluids based on the recent experimental data of quartz solubility by Scheuermann et al. (2018), with the density equation of Fournier (1983) adopted for calculation of dissolved SiO_2(aq). Vapor Cl concentrations at various T-P conditions were calculated based on Driesner and Heinrich (2007) for NaCl-H_2O system. Fig. 6a shows the isothermal lines for vapor/fluid SiO_2(aq)-Cl composition. The data of endmember fluids at Brandon are mostly scattered between 420 and 450 °C. Application to Si-Cl geothermobarometer using the endmember fluid composition of 297 mmol/kg Cl and 9.6 mmol/kg SiO_2(aq), implies subsurface phase separation up to 450 °C and 400 bar (Fig. 6b).

Fe solubility for Brandon vent fluids can be calculated taking explicit account of the newly calibrated T-P of 450 °C and 400 bar. The values of m(Fe) were calculated for different redox buffers as discussed above to constrain the redox condition. At more reduced conditions, fH_2 is required for the calculation (equations [13] and [14]). However, neither fH_2 nor [H_2(aq)] were reported for Brandon vent fluids (Von Damm et al., 2003). Von Damm et al. (2003) did report dissolved H_2S(aq). For sulfur-rich vent fluids formed in basalt hosted hydrothermal systems at deeper levels of oceanic crust, iron sulfides phases (±magnetite) are typically the predominant mineral phases that buffer fluid redox and H_2S (Seyfried and Ding, 1993; German and Seyfried, 2014). Hence, we assume that pyrite-pyrrhotite equilibrium at depth in the ocean crust accounts for the dissolved H_2 and H_2S in Brandon vent fluids, as follows:

$$FeS2(s) + H_2(g) = FeS(s) + H_2S(g),\ K_{H2-H2S} \quad (16)$$

The equilibrium constant $K_{H2\text{-}H2S}$ is calculated as:

$$logK_{H2-H2S} = log\ fH_2S - log\ fH_2 \quad (17)$$

Values of fH_2S were converted from measured dissolved H_2S(aq) using the empirical equation reported by Scheuermann et al. (2020):

$$\ln Y_{H2S-Cl} = 2.512 + 0.009898 \cdot T + 2.462 \cdot \ln\rho + 0.01325 \cdot T \cdot \ln\rho + 5.36 \cdot (\ln\rho)^2 \quad (18)$$

[H_2S(aq)] represents dissolved H_2S(aq) concentration (mmol/kg); T is temperature in °C; $Y_{H2S\text{-}Cl} = fH_2S$ / [H_2S(aq)]. The calculated fH_2 were shown in Fig. 7.

Results show that the measured values of m(Fe) at Brandon are in good agreement with calculated m(Fe) for pyrite-pyrrhotite equilibrium, but are significantly higher than that calculated for hematite-magnetite equilibrium (Fig. 8). The slightly lower values for some data points may be caused by fluid-mixing near the seafloor (Janecky and Seyfried, 1984; German and Seyfried, 2014). The results thus suggest that vent fluids of Brandon hydrothermal field were likely formed in reducing condition in keeping with the PPM-fluid equilibrium. A result such as this is also supported by the calculated fH_2, which is in good agreement with theoretical PPM buffering line (Fig. 7; Table S9). The results demonstrate the effectiveness of the density model developed in the present study in predicting Fe solubility at T-P-ρ_w conditions where HKF model is not directly applicable, greatly expanding our capability of quantitatively constraining fluid-rock equilibrium and metal transport in deep seafloor hydrothermal systems.

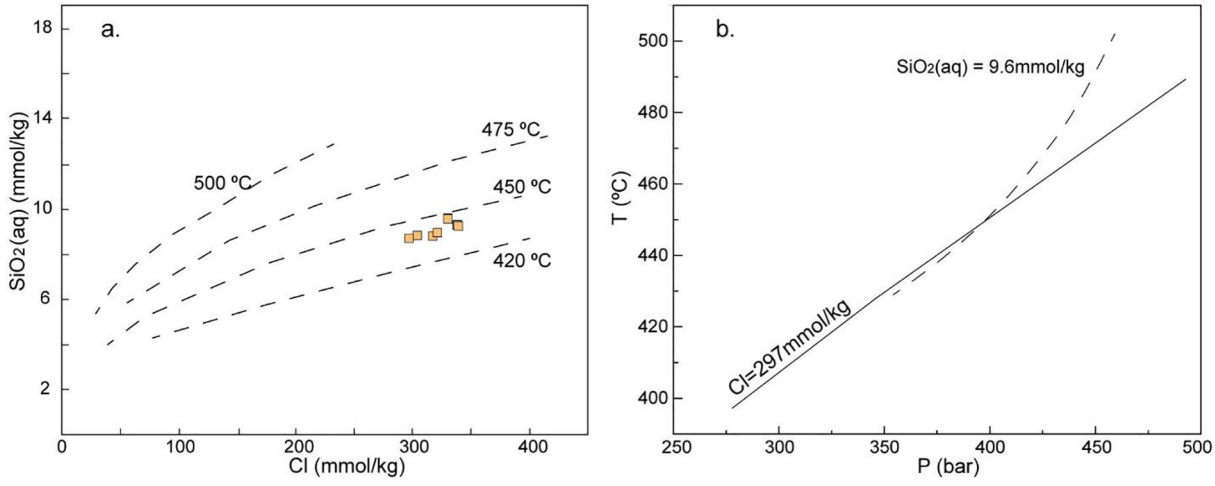

Fig. 6. Estimation of T-P condition of phase separation at Brandon hydrothermal field using Si-Cl geothermobarometer. (a) Dissolved SiO_2(aq) as a function of Cl concentration. Data of endmember vent fluids at Brandon are plotted in colored squares. Dashed lines are isothermal SiO_2-Cl lines calculated using the density model of Fournier (1983). (b) Si-Cl geothermobarometer as applied to the Brandon hydrothermal field using endmember fluid composition, i.e., 297 mmol/kg Cl and 9.6 mmol/kg SiO_2(aq). Fluid Cl iso-concentration line as indicated in solid line is calculated based on Driesner and Heinrich (2007). SiO_2(aq) iso-concentration line as indicated in dashed line is calculated using equation of Fournier (1983). The intersection of Cl and SiO_2(aq) lines suggests T-P of 450 °C and 400 bar.

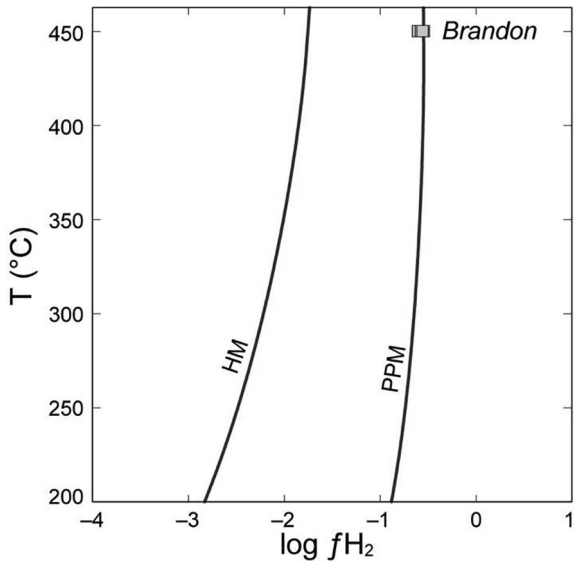

Fig. 7. Diagram showing log fH_2-T relationship of vapor fluids. Solid lines indicate different redox buffers (400 bar). The diagram is constructed using Geochemist's Workbench with thermodynamic data based on updated SUPCRT database.

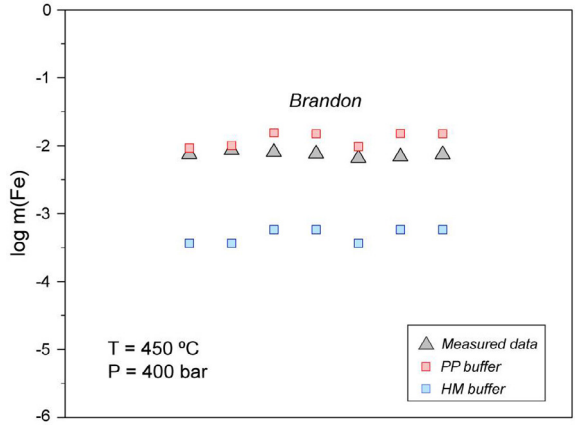

Fig. 8. Measured Fe solubility of Brandon vent fluids compared with values predicted using density model assuming various redox buffers. The equilibrium T-P of Brandon vent fluids were estimated at 450 °C, 400 bar using Si-Cl thermobarometer. Measured values are plotted in gray triangles. Predicted m(Fe) at different redox conditions are shown in colored squares. PP: pyrite-pyrrhotite; HM: hematite-magnetite.

The successful application of the new density model for fluids with density above ~ 0.1 g/cm^3, and temperature up to 500 °C, similar to that constrained by our experiments, is significant. Due to the unusual difficulty of the sample collection during the experiment, uncertainties of T-P measurement may impose relatively large uncertainties in the measured chemical composition, hence the models still need to be improved with further solubility data at similar conditions. Using these models for evaluating Fe solubility in fluids with even lower density (<0.1 g/cm^3) and/or at higher T-P is possible, although this will require experimental data at these conditions using approaches not unlike those outlined in the present contribution.

6. CONCLUSIONS

We report new experimental data for dissolved Fe in vapor-dominated fluid at 400–500 °C and 215–510 bar in equilibrium with KMQ and HM buffers. The new data show that vapor/fluid density and chlorinity are both important factors controlling Fe solubility. Pressure and temperature affect Fe solubility in a complex way by changing density and chlorinity through phase separation. Combining the new experimental data on Fe solubility in low-density fluids (~0.1–0.35 g/cm^3) and the HKF data available in SUPCRT database, an empirical density model was generalized to describe the equilibrium constant for HM buffered Fe solubility reaction, which can then be applied to model Fe in vapor-like low-density hydrothermal fluids. Density models for magnetite dissolution reaction and PPM buffered systems were also determined using this approach. Calculations show that the density model developed in the present study can reproduce well solubility data from previous experimental studies and vent data from seafloor hydrothermal systems, such as Brandon vent (21.5^{0}S, EPR). Combined with the Si-Cl geothermobarometer data, we further suggest that phase separation at Brandon occurs at deeper crustal levels, with peak T-P conditions of phase separation up to 450 °C and 400 bar. The regressed Fe solubility data allow more quantitative redox-related constraints to be placed that origin and evolution of vent fluid chemistry at Brandon, where PPM buffered condition are indicated. From a broad perspective, the new solubility data and the density model developed in this study greatly extend our ability to understand controls on Fe mobility in low-density fluids, when limited experimental data are available. Such information is critical for understanding hydrothermal processes such as phase separation and metal mobility in deep seafloor hydrothermal systems, which are important source of global ocean metal budget.

CREDIT AUTHORSHIP CONTRIBUTION STATEMENT

Yanlu Xing: Conceptualization, Methodology, Investigation, Writing – original draft. **Peter Scheuermann:** Conceptualization, Methodology, Investigation, Writing – original draft. **William E. Seyfried:** Conceptualization, Supervision, Funding acquisition, Writing – review & editing.

Declaration of Competing Interest

The authors declare that they have no known competing financial interests or personal relationships that could have appeared to influence the work reported in this paper.

ACKNOWLEDGEMENT

This research was supported by National Science Foundation (NSF) grant OCE # 1736679 to W.E.S. Dr.

Chunyang Tan helped with building up the pressure vessel and related experimental apparatus. We are grateful to Associate Editor Gleb Pokrovski, and reviewers Artas Migdisov, Maria Kokh and two anonymous reviewers, for their constructive comments and suggestions that help to improve the manuscript significantly.

RESEARCH DATA

Research data can be found within this paper and the Supplementary Material.

APPENDIX A. SUPPLEMENTARY DATA

Supplementary data to this article can be found online at https://doi.org/10.1016/j.gca.2021.09.027.

REFERENCES

Akinfiev N. N. and Diamond L. W. (2003) Thermodynamic description of aqueous nonelectrolytes at infinite dilution over a wide range of state parameters. *Geochim. Cosmochim. Acta* **67**, 613–629.

Anderson G. M. (2005) *Thermodynamics of Natural Systems*. Cambridge University Press, Second..

Anderson G. M., Castet S., Schott J. and Mesmer R. E. (1991) The density model for estimation of thermodynamic parameters of reactions at high temperatures and pressures. *Geochim. Cosmochim. Acta* **55**, 1769–1779.

Bischoff J. and Rosenbauer R. (1987) Phase separation in seafloor geothermal systems; an experimental study of the effects on metal transport. *Am. J. Sci.* **287**, 953–978.

Boctor N. Z., Popp R. K. and Frantz J. D. (1980) Mineral-solution equilibria—IV. Solubilities and the thermodynamic properties of FeCl20 in the system Fe2O3-H2-H2O-HCl. *Geochim. Cosmochim. Acta* **44**, 1509–1518.

Bodnar R. J. and Sterner S. M. (1985) Synthetic fluid inclusions in natural quartz. II. Application to PVT studies. *Geochim. Cosmochim. Acta* **49**, 1855–1859.

Brugger J., Liu W., Etschmann B., Mei Y., Sherman D. M. and Testemale D. (2016) A review of the coordination chemistry of hydrothermal systems, or do coordination changes make ore deposits? *Chem. Geol.* **447**, 219–253.

Butterfield D. A., McDuff R. E., Lilley M. D., Massoth G. J. and Lupton J. E. (1990) Geochemistry of hydrothermal fluids from Axial Seamount Hydrothermal Emissions Study vent field, Juan de Fuca Ridge: Subseafloor boiling and subsequent fluid-rock interaction. *J. Geophys. Res. (United States)* **95**, B8.

Butterfield D. A., McDuff R. E., Mottl M. J., Lilley M. D., Lupton J. E. and Massoth G. J. (1994) Gradients in the composition of hydrothermal fluids from the Endeavour segment vent field: Phase separation and brine loss. *J. Geophys. Res. Solid Earth* **99**, 9561–9583.

Chou I.-M. and Eugster H. (1977) Solubility of magnetite in supercritical chloride solutions. *Am. J. Sci.* **277**, 1296–1314.

Diehl A. and Bach W. (2020) MARHYS (MARine HYdrothermal Solutions) Database: A Global Compilation of Marine Hydrothermal Vent Fluid, End Member, and Seawater Compositions. Geochemistry, Geophys. Geosystems 21, e2020GC009385.

Ding K. and Seyfried W. E. (1992) Determination of Fe-Cl complexing in the low pressure supercritical region (NaCl fluid): Iron solubility constraints on pH of subseafloor hydrothermal fluids. *Geochim. Cosmochim. Acta* **56**, 3681–3692.

Driesner T. and Heinrich C. A. (2007) The system H2O–NaCl. Part I: Correlation formulae for phase relations in temperature–pressure–composition space from 0 to 1000°C, 0 to 5000bar, and 0 to 1 XNaCl. *Geochim. Cosmochim. Acta* **71**, 4880–4901.

Edmonds H. N., German C. R., Green D. R. H., Huh Y., Gamo T. and Edmond J. M. (1996) Continuation of the hydrothermal fluid chemistry time series at TAG, and the effects of ODP drilling. *Geophys. Res. Lett.* **23**, 3487–3489.

Fein J. B., Hemley J. J., D'Angelo W. M., Komninou A. and Sverjensky D. A. (1992) Experimental study of iron-chloride complexing in hydrothermal fluids. *Geochim. Cosmochim. Acta* **56**, 3179–3190.

Fontaine F. J., Wilcock W. S. D., Foustoukos D. E. and Butterfield D. A. (2009) A Si-Cl geothermobarometer for the reaction zone of high-temperature, basaltic-hosted mid-ocean ridge hydrothermal systems. *Geochemistry, Geophys. Geosystems* **10**.

Fournier R. O. (1983) A method of calculating quartz solubilities in aqueous sodium chloride solutions. *Geochim. Cosmochim. Acta* **47**, 579–586.

Foustoukos D. I. and Seyfried W. E. (2007) Fluid Phase Separation Processes in Submarine Hydrothermal Systems. *Rev. Mineral. Geochemistry* **65**, 213–239.

Fowler A. P. G., Scheuermann P., Tan C. and Seyfried W. (2019) Titanium reactors for redox-sensitive hydrothermal experiments: An assessment of dissolved salt on H2 activity-concentration relations. *Chem. Geol.* **515**, 87–93.

Gallant R. M. and Von Damm K. L. (2006) Geochemical controls on hydrothermal fluids from the Kairei and Edmond Vent Fields, 23°-25°S, Central Indian Ridge. *Geochemistry, Geophys. Geosystems* **7**, n/a-n/a.

Gamo T., Chiba H., Masuda H., Edmonds H. N., Fujioka K., Kodama Y., Nanba H. and Sano Y. (1996) Chemical characteristics of hydrothermal fluids from the TAG Mound of the Mid-Atlantic Ridge in August 1994: Implications for spatial and temporal variability of hydrothermal activity. *Geophys. Res. Lett.* **23**, 3483–3486.

German C. R. and Seyfried W. E. (2014) Hydrothermal Processes. In Treatise on Geochemistry pp. 191–233.

Heinrich C. A. and Seward T. M. (1990) A spectrophotometric study of aqueous iron (II) chloride complexing from 25 to 200° C. *Geochim. Cosmochim. Acta* **54**, 2207–2221.

Ho P. C. and Palmer D. A. (1997) Ion association of dilute aqueous potassium chloride and potassium hydroxide solutions to 600°C and 300 MPa determined by electrical conductance measurements. *Geochim. Cosmochim. Acta* **61**, 3027–3040.

Ho P. C., Palmer D. A. and Gruszkiewicz M. S. (2001) Conductivity measurements of dilute aqueous HCl solutions to high temperatures and pressures using a flow-through cell. *J. Phys. Chem. B* **105**, 1260–1266.

Holland T. J. B. and Powell R. (2011) An improved and extended internally consistent thermodynamic dataset for phases of petrological interest, involving a new equation of state for solids. *J. Metamorph. Geol.* **29**, 333–383.

Hurtig N. C. and Williams-Jones A. E. (2014) An experimental study of the solubility of MoO_3 in aqueous vapour and low to intermediate density supercritical fluids. *Geochim. Cosmochim. Acta* **136**, 169–193.

Hurtig N. C. and Williams-Jones A. E. (2015) Porphyry-epithermal Au-Ag-Mo ore formation by vapor-like fluids: New insights from geochemical modeling. *Geology* **43**, 587–590.

Janecky D. R. and Seyfried W. E. (1984) Formation of massive sulfide deposits on oceanic ridge crests: Incremental reaction models for mixing between hydrothermal solutions and seawater. *Geochim. Cosmochim. Acta* **48**, 2723–2738.

Johnson J. W. and Oelkers E. H. (1992) *SUPCRT92: a software package for calculating the standard molal thermodynamic properties of minerals, gases, aqueous species, and reaction from 1 to 5000 bar and 0 to 1000 °C*. Comput, Geosci, p. 18.

Khaibullin I. K. and Borisov N. M. (1966) Experimental investigation of thermal properties of aqueous and vapor solutions of sodium and potassium chlorides at phase equilibrium. *High Temp.* **4**, 489–494.

Kishima N. and Sakai H. (1984) Fugacity-concentration relationship of dilute hydrogen in water at elevated temperature and pressure. *Earth Planet. Sci. Lett.* **67**, 79–86.

Kokh M. A., Lopez M., Gisquet P., Lanzanova A., Candaudap F., Besson P. and Pokrovski G. S. (2016) Combined effect of carbon dioxide and sulfur on vapor–liquid partitioning of metals in hydrothermal systems. *Geochim. Cosmochim. Acta* **187**, 311–333.

Lemire R., Berner U., Musikas C., Palmer D., Taylor P. and Tochiyama O. (2013) Chemical thermodynamics of IRON. OECD Nucl. Energy Agency Data Bank, Eds., North Holl. Elsevier Sci. Publ. B. V., Amsterdam, Netherlands.

Lemke K. H. and Seward T. M. (2018) Molecular Clusters and Solvation in Volcanic and Hydrothermal Vapors. *Rev. Mineral. Geochemistry* **84**, 57–83.

Liu W., Etschmann B., Brugger J., Spiccia L., Foran G. and McInnes B. (2006) UV–Vis spectrophotometric and XAFS studies of ferric chloride complexes in hyper-saline LiCl solutions at 25–90 °C. *Chem. Geol.* **231**, 326–349.

Manning C. E. (1994) The solubility of quartz in H2O in the lower crust and upper mantle. *Geochim. Cosmochim. Acta* **58**, 4831–4839.

Manning C. E. (2013) Thermodynamic Modeling of Fluid-Rock Interaction at Mid-Crustal to Upper-Mantle Conditions. *Rev. Mineral. Geochemistry* **76**, 135–164.

McCollom T. M. and Seewald J. S. (2003) Experimental constraints on the hydrothermal reactivity of organic acids and acid anions: I. Formic acid and formate. *Geochim. Cosmochim. Acta* **67**, 3625–3644.

McDermott J. M., Sylva S. P., Ono S., German C. R. and Seewald J. S. (2018) Geochemistry of fluids from Earth's deepest ridge-crest hot-springs: Piccard hydrothermal field. *Mid-Cayman Rise. Geochim. Cosmochim. Acta* **228**, 95–118.

Mei Y., Liu W., Sherman D. M. and Brugger J. (2014) Metal complexation and ion hydration in low density hydrothermal fluids: Ab initio molecular dynamics simulation of Cu(I) and Au(I) in chloride solutions (25–1000°C, 1–5000bar). *Geochim. Cosmochim. Acta* **131**, 196–212.

Migdisov A. A. and Williams-Jones A. E. (2013) A predictive model for metal transport of silver chloride by aqueous vapor in ore-forming magmatic-hydrothermal systems. *Geochim. Cosmochim. Acta* **104**, 123–135.

Ohmoto H., Hayashi K.-I. and Kajisa Y. (1994) Experimental study of the solubilities of pyrite in NaCl-bearing aqueous solutions at 250–350°C. *Geochim. Cosmochim. Acta* **58**, 2169–2185.

Pester N. J., Ding K. and Seyfried W. E. (2015) Vapor–liquid partitioning of alkaline earth and transition metals in NaCl-dominated hydrothermal fluids: An experimental study from 360 to 465 °C, near-critical to halite saturated conditions. *Geochim. Cosmochim. Acta* **168**, 111–132.

Pokrovski G. S., Borisova A. Y. and Bychkov A. Y. (2013) Speciation and Transport of Metals and Metalloids in Geological Vapors. *Rev. Mineral. Geochemistry* **76**, 165–218.

Pokrovski G. S., Borisova A. Y. and Harrichoury J.-C. (2008) The effect of sulfur on vapor–liquid fractionation of metals in hydrothermal systems. *Earth Planet. Sci. Lett.* **266**, 345–362.

Pokrovski G. S., Roux J. and Harrichoury J.-C. (2005a) Fluid density control on vapor-liquid partitioning of metals in hydrothermal systems. *Geology* **33**, 657–660.

Pokrovski G. S., Roux J., Hazemann J. L. and Testemale D. (2005b) An X-ray absorption spectroscopy study of argutite solubility and aqueous Ge(IV) speciation in hydrothermal fluids to 500 °C and 400 bar. *Chem. Geol.* **217**, 127–145.

Proust P. and Vera J. H. (1989) PRSV: The stryjek-vera modification of the peng-robinson equation of state. Parameters for other pure compounds of industrial interest. *Can. J. Chem. Eng.* **67**, 170–173.

Scheuermann P. P., Tan C. and Seyfried W. E. (2018) Quartz Solubility in the Two-Phase Region of the NaCl-H2O System: An Experimental Study With Application to the Piccard Hydrothermal Field, Mid-Cayman Rise. *Geochemistry. Geophys. Geosystems* **19**, 3570–3582.

Scheuermann P. P., Tutolo B. M. and Seyfried W. E. (2019) Anhydrite solubility in low-density hydrothermal fluids: Experimental measurements and thermodynamic calculations. *Chem. Geol.* **524**, 184–195.

Scheuermann P. P., Xing Y., Ding K. and Seyfried W. E. (2020) Experimental measurement of H2(aq) solubility in hydrothermal fluids: Application to the Piccard hydrothermal field. *Mid-Cayman Rise. Geochim. Cosmochim. Acta* **283**, 22–39.

Scholten L., Schmidt C., Lecumberri-Sanchez P., Newville M., Lanzirotti A., Sirbescu M.-L.-C. and Steele-MacInnis M. (2019) Solubility and speciation of iron in hydrothermal fluids. *Geochim. Cosmochim. Acta* **252**, 126–143.

Seyfried W. E. and Ding K. (1995) *Phase Equilibria in Subseafloor Hydrothermal Systems: a Review of the Role of Redox, Temperature, Ph and Dissolved Cl on the Chemistry of Hot Spring Fluids at Mid-Ocean Ridges*. Physical, Chemical, Biological, and Geological Interactions, In Seafloor Hydrothermal Systems, pp. 248–272.

Seyfried W. E. and Ding K. (1993) The effect of redox on the relative solubilities of copper and iron in Cl-bearing aqueous fluids at elevated temperatures and pressures: An experimental study with application to subseafloor hydrothermal systems. *Geochim. Cosmochim. Acta* **57**, 1905–1917.

Seyfried W. E., Pester N. J., Ding K. and Rough M. (2011) Vent fluid chemistry of the Rainbow hydrothermal system (36°N, MAR): Phase equilibria and in situ pH controls on subseafloor alteration processes. *Geochim. Cosmochim. Acta* **75**, 1574–1593.

Seyfried W. E., Seewald J. S., Berndt M. E., Ding K. and Foustoukos D. I. (2003) *Chemistry of hydrothermal vent fluids from the Main Endeavour Field, northern Juan de Fuca Ridge: Geochemical controls in the aftermath of June 1999 seismic events*. J. Geophys. Res, Solid Earth, p. 108.

Simon A. C., Pettke T., Candela P. A., Piccoli P. M. and Heinrich C. A. (2004) Magnetite solubility and iron transport in magmatic-hydrothermal environments. *Geochim. Cosmochim. Acta* **68**, 4905–4914.

Stefánsson A., Lemke K. H. and Seward T. M. (2019) Iron(III) chloride complexation in hydrothermal solutions: A combined spectrophotometric and density functional theory study. *Chem. Geol.* **524**, 77–87.

Stryjek R. and Vera J. H. (1986) PRSV: An improved peng—Robinson equation of state for pure compounds and mixtures. *Can. J. Chem. Eng.* **64**, 323–333.

Sverjensky D. A., Shock E. L. and Helgeson H. C. (1997) Prediction of the thermodynamic properties of aqueous metal complexes to 1000°C and 5 kb. *Geochim. Cosmochim. Acta* **6**, 1359–1412.

Tagirov B. R., Zotov A. V and Akinfiev N. N. (1997) Experimental study of dissociation of HCl from 350 to 500°C and from 500 to

2500 bars: Thermodynamic properties of HCl°(aq). Geochim. Cosmochim. Acta 61, 4267–4280.

Tanger J. C. and Helgeson H. C. (1988) Calculation of the thermodynamic and transport properties of aqueous species at high pressures and temperatures: Revised equations of state for the standard partial molal properties of ions and electrolytes. *Am. J. Sci.* **288**, 19–98.

Testemale D., Brugger J., Liu W., Etschmann B. and Hazemann J.-L. (2009) In-situ X-ray absorption study of Iron(II) speciation in brines up to supercritical conditions. *Chem. Geol.* **264**, 295–310.

Tremaine P. R. and LeBlanc J. C. (1980) The solubility of magnetite and the hydrolysis and oxidation of Fe2+ in water to 300°C. *J. Solution Chem.* **9**, 415–442.

Velizhanin K. A., Alcorn C. D., Migdisov A. A. and Currier R. P. (2020) Rigorous analysis of non-ideal solubility of sodium and copper chlorides in water vapor using Pitzer-Pabalan model. *Fluid Phase Equilib.* **522** 112731.

Von Damm K. L., Edmond J. M., Grant B., Measures C. I., Walden B. and Weiss R. F. (1985) Chemistry of submarine hydrothermal solutions at 21 °N. *East Pacific Rise. Geochim. Cosmochim. Acta* **49**, 2197–2220.

Von Damm K. L., Lilley M. D., Shanks W. C., Brockington M., Bray A. M., O'Grady K. M., Olson E., Graham A. and Proskurowski G. (2003) Extraordinary phase separation and segregation in vent fluids from the southern East Pacific Rise. *Earth Planet. Sci. Lett.* **206**, 365–378.

Von Damm K. L., Oosting S. E., Kozlowski R., Buttermore L. G., Colodner D. C., Edmonds H. N., Edmond J. M. and Grebmeier J. M. (1995) Evolution of East Pacific Rise hydrothermal vent fluids following a volcanic eruption. *Nature* **375**, 47–50.

Williams-Jones A. E. and Heinrich C. A. (2005) Vapor Transport of Metals and the Formation of Magmatic-Hydrothermal Ore Deposits. *Econ. Geol.* **100**, 1287–1312.

Xing Y., Etschmann B., Liu W., Mei Y., Shvarov Y., Testemale D., Tomkins A. and Brugger J. (2019) *The role of fluorine in hydrothermal mobilization and transportation of Fe*. U and REE and the formation of IOCG deposits. Chem, Geol, p. 504.

Ziemniak S. E., Jones M. E. and Combs K. E. S. (1995) Magnetite solubility and phase stability in alkaline media at elevated temperatures. *J. Solution Chem.* **24**, 837–877.

Zotov A. V., Kuzmin N. N., Reukov V. L. and Tagirov B. R. (2018) Stability of $AuCl_2^-$ from 25 to 1000 °C at Pressures to 5000 bar and Consequences for Hydrothermal Gold Mobilization. *Miner.* **8**.

Associate Editor: Gleb S. Pokrovski